Development of a Fast-Swimming Dolphin Robot Capable of Leaping

Junzhi Yu, *Senior Member, IEEE*, Zongshuai Su, Zhengxing Wu, and Min Tan

***Abstract*—It remains a great challenge for a biomimetic dolphin robot to leap out of the water by reason of requirements for very high speed and exquisite motion control. In this paper, we estimate the minimum exit speed that allows the dolphin to completely leap out of the water, and for the first time, we build a self-contained leaping dolphin robot with commercially available actuators and power supply. To quantify the possible impact of the body length on the minimum exit speed during the leap, we employ a rigid body model rather than a particle model to numerically evaluate the leaping process. Furthermore, a robotic prototype intended for leap motions is created, with particular emphasis on streamlining and high-thrust tail propulsive mechanism designs in conjunction with a passive control strategy for the dorsoventral propulsion. Underwater tests on the untethered dolphin robot demonstrate the effectiveness of the proposed methods and mechatronic designs. We found that the dolphin robot successfully performed leaps with a length-specific speed of over 2.3 body lengths per second, and an emergence angle ranging between 35 and 60°.**

***Index Terms*—Bioinspired robot, control engineering, dolphin robot, leaping, minimum exit speed.**

I. Introduction

BIOINSPIRED robots have drawn a great deal of interest from the robotics and biology community over the past decades [1]–[7]. In particular, much attention has been paid to understanding and replicating the propulsive principles of marine animals like cetacean and fish. As typical cetaceans, dolphins are characterized as high-speed and agile swimmers. They can swim at speeds up to 11.1 m/s (equivalent to 6.0 body lengths/s, hereafter abbreviated as BL/s), and even jump to heights of over 5 m above water, sometimes with one or two flips or spirals in the air [8], [9]. These amazing locomotion techniques provide a great variety of sources of inspiration for robot design. The potential benefits of biomimetic dolphin-like propulsion applied to autonomous underwater vehicle (AUV) design would involve high speed, energy economy, enhanced maneuverability, or reduced detection [10]. Meanwhile, leaping dolphin robot may be able to fulfill some aquatic-related tasks such as exploration, reconnaissance, transportation, and cross-media sensing.

A running mode in dolphin swimming, also known as "porpoising," consisting of rhythmic, serial leaps out of the water [11]. To clear the water, dolphins must achieve sufficient underwater speed and momentum to overcome the influence of gravity when they leave the water. According to documented porpoising speeds, a small leap for dolphins (*Stenella spp.*) typically occurred at speeds ranging from 3.6 to 4.6 m/s [12], while maximum speeds for *Tursiops truncatus* swimming upwards, prior to vertical leaps varied from 8.2 to 11.2 m/s [13]. There has been considerable interest from both theoretical models and practical experiments to explore mechanics and control of high-speed swimming by dolphins [14], [15]. Since undisturbed experimental verification on wild free-ranging dolphins is difficult to accomplish directly, a possible alternative is to develop a fast-swimming and maneuverable dolphin robot for repeatable evaluation, serving as a test bed for research on dolphin-like locomotion. More importantly, it is curious to know what is the minimum speed a dolphin must have to initiate a leap.

The key challenge faced by the researchers in the fields of biomimetic dolphin robots is to accommodate daunting speed and control requirements of sideward and even vertical leaps. In practice, there have been a lot of studies on dolphin robots in the context of biorobotics. Many issues have been investigated, such as propulsion modeling [16], [17], thrust optimization [18], yaw and pitch maneuvering control [19], and real-world application to water quality monitoring [20]. In the meantime, several robotic prototypes have been developed, e.g., Nakashima's two-joint dolphin with a pair of 1-degree of freedom (DOF) pectoral fins and a dorsal fin in which one joint is driven by a dc motor and the other is passive [21], [22], Dogangil's four-link dolphin robot driven by pneumatic actuators [23], a five-link dolphin robot with a pair of 2-DOF flippers [16], a two-motor-driven Scotch yoke robotic dolphin characterized by its online adjustable oscillatory amplitude [24], a dolphin robot capable of 3-D swimming with a mechanical slider [25], and a slider-crank centered self-propelled dolphin robot [26]. These prototypes primarily utilized a multilink-based mechanism for a primary thrust generator. Furthermore, taking the maximum length-specific cruising speed as an assessment, Nakashima's two-generation dolphin robots reached speeds of up to 0.62 BL/s and 0.95 BL/s, respectively [21]; Dogangil's dolphin robot peaked 0.5 BL/s [23], and Yu's two dolphin robots attained 0.63 BL/s [16] and 1.05 BL/s [26], respectively. These collected data indicate that

Manuscript received December 26, 2015; revised March 28, 2016; accepted May 12, 2016. Date of publication May 25, 2016; date of current version October 13, 2016. Recommended by Technical Editor M. Basin. This work was supported in part by the National Natural Science Foundation of China under Grant 61375102, Grant 61333016, and Grant 61421004; in part by the Beijing Natural Science Foundation under Grant 3141002 and Grant 4161002; and in part by the National Defense Science and Technology Innovation Fund of the Chinese Academy of Sciences under Grant CXJJ-16M110. *(Corresponding author: Junzhi Yu.)*

The authors are with the State Key Laboratory of Management and Control for Complex Systems, Institute of Automation, Chinese Academy of Sciences, Beijing 100190, China (e-mail: junzhi.yu@ia.ac.cn; zongshuai.su@ia.ac.cn; zhengxing.wu@ia.ac.cn; min.tan@ia.ac.cn).

Color versions of one or more of the figures in this paper are available online at http://ieeexplore.ieee.org.

Digital Object Identifier 10.1109/TMECH.2016.2572720

1083-4435 © 2016 IEEE. Personal use is permitted, but republication/redistribution requires IEEE permission.
See http://www.ieee.org/publications_standards/publications/rights/index.html for more information.

the maximum propulsive speed achieved so far is around 1 BL/s. Therefore, more powerful and structurally robust mechanisms are demanded to significantly boost the propulsive performance of dolphin robots.

For the purpose of performing leaps on a robotic platform, in this paper, we focus mainly on several critical design details that attempt to maximize propulsive speed during locomotion. First, we carefully estimate the minimum exit speed of a dolphin robot intended to launch a leap by using a rigid body model rather than an overly simplified particle model. Second, a propulsive scheme synthesizing streamlining, material, propulsive mechanism, and control strategy is proposed and implemented. Compared with the previously reported dolphin robots, the created dolphin robot attained a markedly larger speed topping 2.85 BL/s. Being able to execute leaps is another distinctive feature for this fast-swimming and maneuverable swimming robot. To the best of our knowledge, this is the first time that leap motions have been successfully performed on a physical dolphin robot.

The remainder of this paper is organized as follows. We start by estimating the minimum exit speed for initiating a leap in Section II. We then proceed to develop a free-swimming dolphin robot intended for leap motions in Section III. The aquatic experiments on the fully untethered dolphin robot and related discussion are offered in Section IV. Finally, concluding remarks are given in Section V.

II. Numerical Estimation of the Minimum Exit Speed

In an effort to make dolphin robots swim faster, our aim is to exploit this speed to leap out of the water. To guide the design of a dolphin robot with a body length (L), foremost is the determination of an initial exit speed (U_0) at the moment of penetrating the water surface for an entire leap with a varying emergence angle (α), which is seldom addressed in the literature. With the purpose of quantifying the possible effect of the body length on the minimum exit speed ($U_{0\min}$) during the leap, we numerically evaluate the leaping process. Unlike existing biological leaping models in which the animal is treated as a particle (or point mass) [27], [28], the dolphin robot is viewed as a rigid body with a certain length in our model. Again, in comparison with our prior work that proposed a dynamic porpoising model for a multilink dolphin-like robot [29], the current model is based on the force equilibrium equations instead of the energy conservation equations, enabling further mechanical parameter estimation.

An entire leaping process, as illustrated in Fig. 1, can be divided into five distinct phases:

1) an acceleration phase, which is characterized by large-thrust swimming motions at almost constant depth;
2) a surfacing phase, featuring as rapid ascent before breaking the water surface;
3) a takeoff phase, starting from the emergence of the tip of rostrum till the vertical component of propulsive velocity becoming zero;
4) a flight phase, following an approximate ballistic path in the air above water surface;

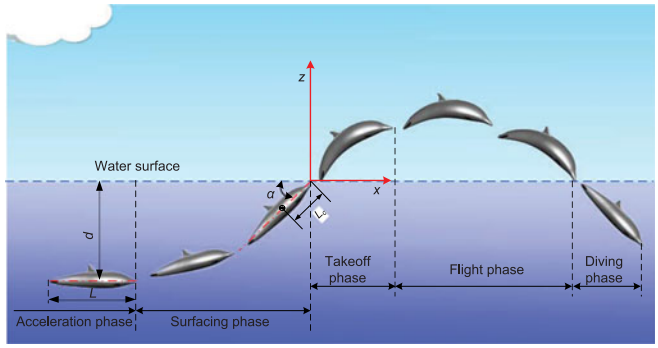

Fig. 1. Schematic illustration of an entire dolphin leap.

5) a diving phase, during which reentering the water head-first takes place.

Note that body length (L) is measured from the tip of rostrum to fluke notch, and that submersion depth (d) is measured from the water surface to the centerline of the dolphin body.

To evaluate the minimum exit speed at the moment of penetrating the water surface, we built a numerical dynamical model of dolphin leaping. In particular, we restrict our analysis to the takeoff phase where the dolphin is becoming airborne till the vertical component of propulsive velocity decreases to zero. In the interest of simplicity, two hypotheses are made.

1) Hypothesis 1: The total thrust generated by the caudal peduncle (i.e., fluke) remains constant before the fluke fully leaving the water [11], [27].
2) Hypothesis 2: During crossing the water–air interface, increased wave drag and decreased pressure drag to a large degree cancel out.

Wave drag will increase because the shock waves around the dolphin body become much stronger. By contrast, the pressure drag will decrease since the head has been out of the water. Moreover, the whole leaping process lasts a very short time and the gravity becomes dominant at the later stage of leaping process. Thus, we suppose that these drags such as wave drag and pressure drag can cancel out, and that the total drags can be calculated in the same way when the dolphin robot swims under water. It follows that the change of drag forces undergone by the dolphin is solely associated with the forward speed. Therefore, the motion equation of the dolphin described by its center of mass (COM) can further be formulated, enabling numerical simulation of different leaps.

As shown in Fig. 2, we make direct use of force equilibrium equations to indicate the state of the dolphin. Note that air resistance is assumed to have a negligible effect as the dolphin rises and falls. For the forces in the horizontally forward (x) and vertical (z) directions, it follows that:

$$\begin{cases} T\cos\alpha - D_f\cos\alpha = (1+m)M\ddot{x} \\ T\sin\alpha - D_f\sin\alpha - G_f = (1+m)M\ddot{z} \end{cases} \tag{1}$$

where T indicates the thrust provided by dorsoventral oscillations of the posterior body and fluke; D_f is the resistance at the water-air interface; G_f is the gravity contributed by the emerged

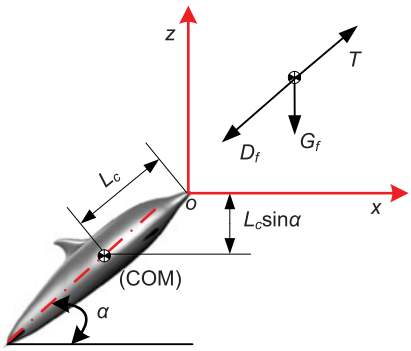

Fig. 2. Schematic representation of forces on an emerging dolphin.

part of the dolphin in the air; m is a correlation term about the added mass of the dolphin robot, accounting for the spray carried along with the leaping dolphin as it emerges [11]; M is the total body mass; L_c is the distance between the center of mass and the rostrum along the longitudinal axis of dolphin body; and $\ddot{x}$ and $\ddot{z}$ are the accelerations in the x- and z-directions, respectively.

According to Hypothesis 2, we have

$$D_f = D_0 \frac{U^2}{{U_0}^2} = D_0 \frac{\dot{x}^2}{{U_0}^2 \cos^2\alpha} \tag{2}$$

where D_0 is the initial drag and U is the linear velocity along the advancement direction. Replacing D_f in the first equation of (1), it immediately follows that:

$$T\cos\alpha - D_0 \frac{\dot{x}^2}{{U_0}^2 \cos\alpha} = (1+m)M\ddot{x}. \tag{3}$$

Clearly, this equation is equivalent to the dynamic equation in steady dolphin swimming, which only has the trivial solution $\ddot{x} \equiv 0$. That is, the horizontal speed of the dolphin remains constant throughout the takeoff phase. Hence, we easily obtain $t_1 = L/U_0$ and $T = D_f$, where t_1 indicates the time interval between the onset of the tip of rostrum leaving the water and the onset of the fluke leaving the water.

Further considering that gravity, being a vertical force, affects only the vertical motion, the second equation of (1) can be simplified as $-G_f = (1+m)M\ddot{z}$. Here, G_f is a function of the total mass, i.e., $G_f = \lambda(l)Mg$, where $\lambda(l) \in [0,1]$ is defined as the ratio of the mass for the emerged part to the total body mass and l is the length of the emerged dolphin body. Since the dolphin body takes a fusiform shape, meaning that the animal is wide in the middle but tapered at each end according to the slender body theory [30], $\lambda(l)$ can mathematically be written as $\lambda(l) = -2(\frac{l}{L})^3 + 3(\frac{l}{L})^2$. A plot of the mass ratio (λ) against the body length (l) is illustrated in Fig. 3. Then, the second equation of (1) becomes

$$-\lambda(l)Mg = (1+m)M\ddot{z} \tag{4}$$

and hence

$$\ddot{z} = \frac{g}{1+m}\left(\frac{2}{L^3}{U_0}^3 t^3 - \frac{3}{L^2}{U_0}^2 t^2\right). \tag{5}$$

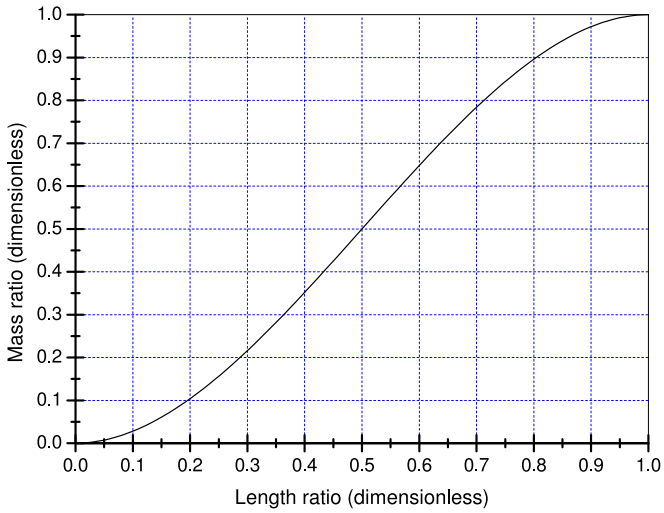

Fig. 3. Plot of the mass ratio against the body length.

Apparently, the initial condition is $\begin{cases} \dot{z}(0) = U_0 \sin\alpha \\ z(0) = -L_c \sin\alpha \end{cases}$. By integrating this equation with respect to time once to yield velocity and twice to yield displacement, we obtain

$$\begin{cases} \dot{z} = \dfrac{g}{1+m}\left(\dfrac{1}{2L^3}{U_0}^3 t^4 - \dfrac{1}{L^2}{U_0}^2 t^3\right) \\ \qquad + U_0 \sin\alpha \\ z = \dfrac{g}{1+m}\left(\dfrac{1}{10L^3}{U_0}^3 t^5 - \dfrac{1}{4L^2}{U_0}^2 t^4\right) \\ \qquad + U_0 t \sin\alpha - L_c \sin\alpha. \end{cases}, \quad t \in [0, t_1] \tag{6}$$

With the aid of the previously formulated dynamic analysis, we numerically estimated the minimum exit speeds at three different emergence angles of 30°, 45°, and 60° with a wide range of body lengths. During simulations, the judgment condition of an entire leap is defined as $z - \frac{L}{9} \geq 0$, with the minimum exit height being the distance between the COM and the venter of the dolphin calculated by $H_{\min} = \frac{D}{2} = \frac{\frac{L}{4.5}}{2} = \frac{L}{9}$. Particularly, we traverse $t \in [0,2]$, $U_0 \in [0,5L]$, and $\alpha \in [30°, 60°]$ with a small step to find a minimum U_0 till $z - \frac{L}{9} \geq 0$ is satisfied, where the added mass coefficient m is roughly 0.2 [31]. Note that the majority of the body leaves the water surface and the posterior body does not contribute to thrust production any longer at the end of the takeoff phase. At this moment, instead of upward oscillations, the dolphin flaps its posterior body downward and simultaneously jerks down its neck joint to assume a C-shape, thereby yielding a sufficient nose-down pitching moment which helps enforce reentry into the water.

The calculated minimum exit speeds against body lengths are shown in Fig. 4. Given the maximum leap height (H) being $H = (U_0 \sin\alpha)2/2g$ according to conservation of energy, increasing α theoretically brings a significant improvement in maximum leap height. That is, a dolphin leaping and diving at

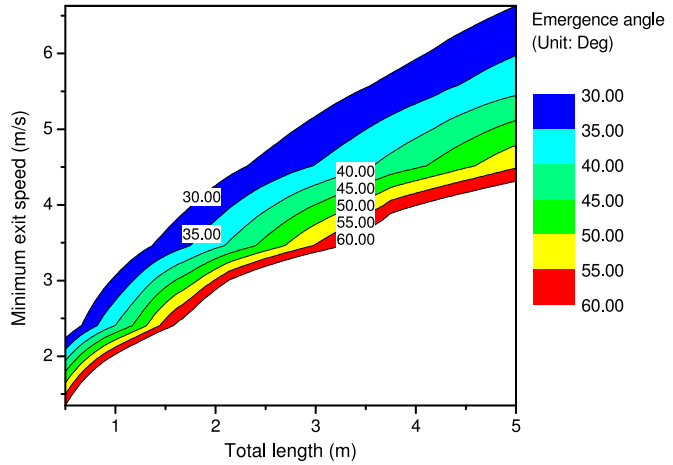

Fig. 4. Filled contour plot of minimum exit speeds against different body lengths.

a larger α reduces its forward speed, but improves its opportunities of entirely elevating the body out of the water surface with a relatively low $U_{0\min}$. This trend is revealed in Fig. 4, implying that emergence angle is a compromise between that for minimum exit speed and that for maximum forward speed. To ensure the robot to leave the water surface with ease, an emergence angle of 60° that is larger than conventionally hypothesized 45° [11], [27] is preset to compute $U_{0\min}$ in leaping estimation. A 0.7-m-long robot, for example, needs a minimum exit speed of 1.60 m/s (corresponding to 2.29 BL/s) to launch a leap.

III. Mechatronic Design of Leaping-Oriented Dolphin Robot

Using the estimated minimum exit speed as a guide, we build a dolphin robot for leap motions. To facilitate design and fabrication of the robot with commercially available parts, a body length of around 70 cm is chosen. A recent study on hydrodynamic force measurement of swimming dolphins suggests that a culmination of muscle power and streamlining rather than a special drag-reduction mechanism allows dolphins to reach high speeds in a viscous environment like water [32]. Although mass factors are out in the previous numerical calculation, it may still be essential as biological dolphins theoretically need to generate a thrust-to-weight ratio of at least 1:1 for leaping motions. Thus, we focus on high-thrust tail propulsive mechanism designs and streamlining without recourse to specialized appendages.

A. Power Estimation for the Caudal Joint

This subsection gives a detailed description about the power estimation for the caudal joint so as to choose a suitable driving motor. The fluke is a major source of thrust generation in dolphin swimming. According to the biological studies on dolphin swimming [9], we suppose that the length of the peduncle is $L_p = \frac{L}{3}$ and the oscillatory amplitude of fluke is $A = 0.2\ L$.

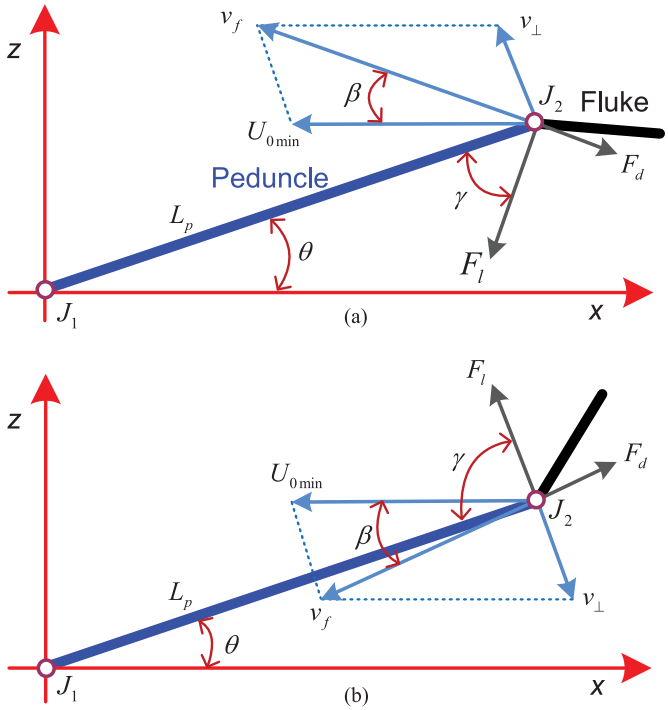

Fig. 5. Illustrations of power estimation. (a) Peduncle oscillates from the central axis to the top point. (b) Peduncle oscillates from the top point to the central axis.

Thus, the amplitude of the caudal joint is computed as

$$\Lambda = \arcsin \frac{A}{L_p}. \tag{7}$$

The joint angle of the caudal joint is

$$\theta = \Lambda \sin(2\pi f_0 t) \tag{8}$$

and the angle rate is

$$\dot{\theta} = 2\pi f_0 \Lambda \cos(2\pi f_0 t) \tag{9}$$

where f_0 is the oscillatory frequency of the peduncle. Typically, a biological dolphin is able to swim even more than 0.9 BL in a single oscillation period. For the robot, we conservatively assume that a medium distance, e.g., 0.6 BL can be covered. Hence, $f_0 = U_{0\min}/L/0.6$ is simply set in the following estimation.

Consider the first quarter period $t \in [0, T/4]$ in which the peduncle moves from the central axis to the top point [see Fig. 5(a)], where T is the oscillation period of the peduncle. The speed of the fluke in the dolphin coordinates is $v_\perp = \dot{\theta} L_p$. Thus, its speed in the world coordinates is

$$v_f = \sqrt{(v_\perp \sin\theta + U_{0\min})^2 + (v_\perp \cos\theta)^2}, t \in [0, T/4]. \tag{10}$$

Apparently, the lift force and drag force of the fluke is

$$F_l = \frac{1}{2} C_l \rho S v_f^2 \tag{11}$$

and

$$F_d = \frac{1}{2} C_d \rho S v_f^2 \tag{12}$$

where $\rho = 1000$ kg/m^3 is the density of water and S is the area of the fluke. C_l and C_d are the lift and drag coefficients, respectively. Let

$$\beta = \arctan \frac{v_\perp \cos\theta}{v_\perp \sin\theta + U_{0\min}}, t \in [0, T/4] \tag{13}$$

be the angle between v_f and $U_{0\min}$, then the angle between F_l and the peduncle becomes $\gamma = \frac{\pi}{2} - \beta - \theta$. Therefore, the torque of the caudal joint in the first quarter period can be calculated as

$$\tau = F_d L_p |\cos\gamma| + F_l L_p |\sin\gamma|, t \in [0, T/4]. \tag{14}$$

Similarly, from Fig. 5(b), we have

$$v_f = \sqrt{(v_\perp \sin\theta - U_{0\min})^2 + (v_\perp \cos\theta)^2}, t \in (T/4, T/2] \tag{15}$$

and

$$\beta = \arctan \frac{v_\perp \cos\theta}{v_\perp \sin\theta - U_{0\min}}, t \in (T/4, T/2]. \tag{16}$$

The angle between F_l and the peduncle is $\gamma = \frac{\pi}{2} - \beta + \theta$. Thus, the torque of the caudal joint in the second quarter period is computed as

$$\tau = F_d L_p |\cos\gamma| + F_l L_p |\sin\gamma|, t \in [T/4, T/2]. \tag{17}$$

Finally, ignoring the resistance induced by the peduncle, the instantaneous power of the caudal joint over the first half period is estimated as

$$P = \tau \cdot \dot{\theta}, t \in [0, T/2]. \tag{18}$$

For the convenience of model verification and comparison, the feature parameters applied to power estimation are listed as follows: $L = 0.7$ m, $U_{0\min} = 1.60$ m/s, and $f_0 = U_{0\min}/L/0.6 = 3.81$ Hz. In particular, considering that the angle of attack of the fluke cannot be maintained at 15° through the whole period, the lift and drag coefficients are conservatively estimated as $C_l = 1.0$ and $C_d = 0.015$ at an angle of attack of 10° [33]. According to the biological study [9], the area of the fluke can empirically be estimated as $S = 0.017 L^{1.946} = 0.008492$ m^2. Fig. 6 illustrates the instantaneous power of the caudal joint over the first half period. Specifically, the average power can be calculated as $\bar{P} = \frac{2}{T} \int_0^{\frac{T}{2}} P dt = 73.1$ W. Based on an overall consideration of power, weight, and cost, a power-dense 90-W brushless dc motor (Maxon EC-4pole) is selected to drive the caudal joint, ensuring the high swimming velocity needed in the leaping maneuver. It should be remarked that the instantaneous power output of the caudal joint peaks approximately 150 W according to Fig. 6, which is much lower than the starting power up to 1092 W. In this sense, a 90-W motor is an appropriate candidate for laboratory studies.

B. Propulsion System Configuration

Dolphins propel themselves by dorsoventral oscillations of the posterior body and flukes, accompanied by accurate adjustment of the angles of attack of the flukes. Hence, at least two degrees of freedom are required for the posterior body for the purpose of dorsoventral propulsion. To reduce structural complexity, the dolphin robot is designed to merely possess two propulsive joints (i.e., waist joint J_1 and caudal joint J_2) and one pitching joint (J_0) functioning as neck. Since the primary objective is to pursue high speed, no yaw joint is included to strike a tradeoff between the functionality and the mass. This design certainly limits the yaw maneuverability of the robot. At present, the yaw maneuver can only be achieved by the combination of the fluke and a pair of 2-DOF mechanical flippers under the circumstances.

More specifically, as shown in Fig. 7, we loosely mimic a spotted dolphin (*Stenella attenuate*, a fast swimmer able to reach a length-specific speed of 6.0 BL/s over short distances [35]) in shape at a reduced scale, with a premise that such a biological morphology will hydrodynamically perform well. The fineness ratio of the fusiform body being 5.2 is a good balance between the mechanical assembly requirement and the optimal parameter value of 4.56 [9]. The control surfaces including dorsal fin, flippers, and fluke are fabricated based on the NACA0018 airfoil (see Fig. 8), which is able to maintain thrust at an angle of attack of over 15° [36]. Two 90-W dc motors with different reduction ratios are chosen to drive J_1 and J_2. The moving ranges of J_1 and J_2 are ±17° and ±33° with respect to the x-axis, respectively. So the robot is expected to achieve high-frequency

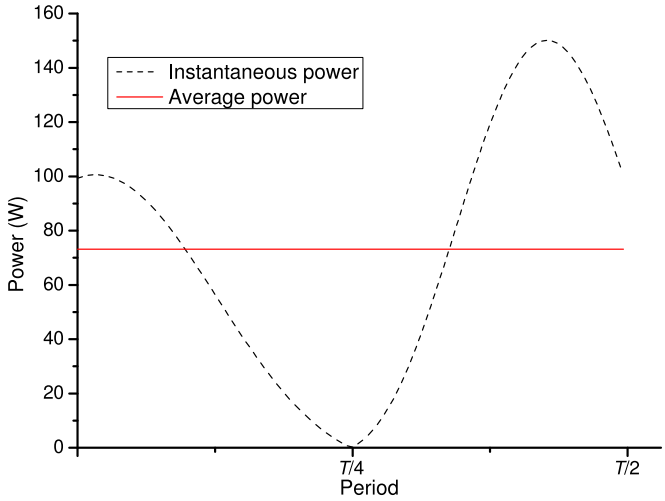

Fig. 6. Instantaneous power of the caudal joint over the first half oscillation period.

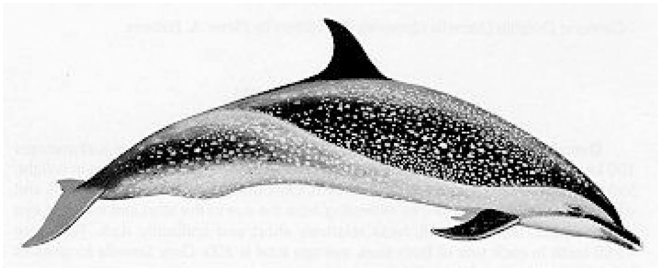

Fig. 7. Referenced spotted dolphin. Adapted from [34].

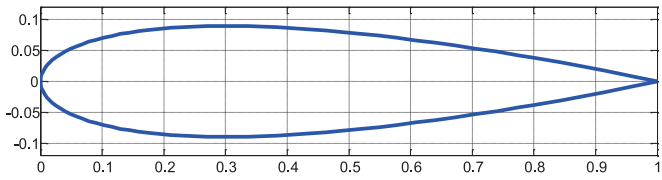

Fig. 8. Symmetric airfoil NACA0018 used for the fluke, flippers, and dorsal fin. Notice that maximum thickness is 18% at 30% chord.

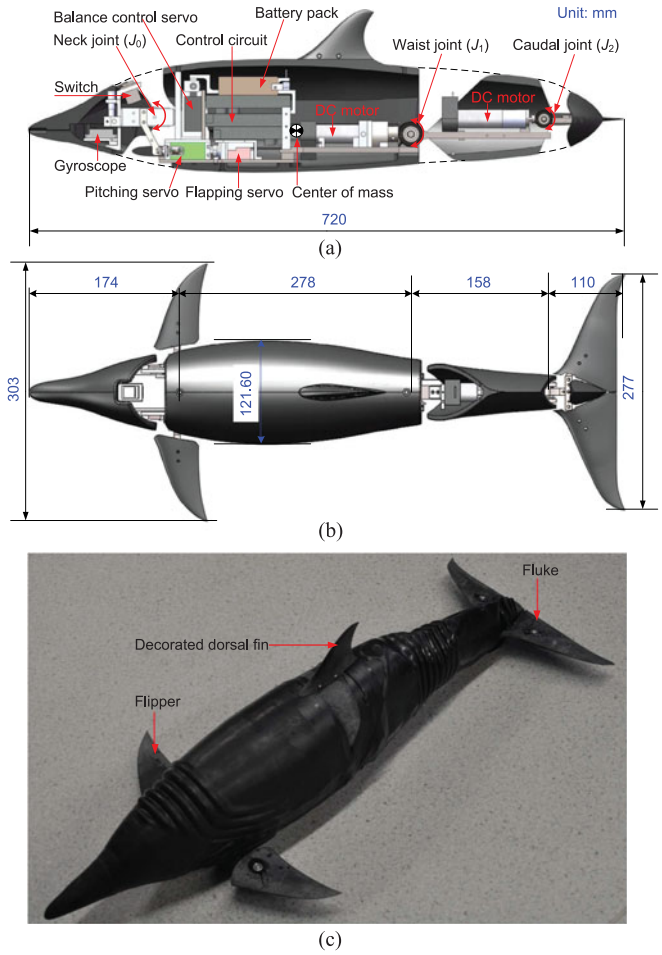

Fig. 9. Overview of the dolphin robot design. (a) Side view of the mechanical propulsion configuration. (b) Top view of the designed robot. (c) Robotic prototype. The forebody is made of polypropylene, while the tail skeleton and interior support bracket are fabricated from titanium alloy, jointly making the robot as light as possible. Sensors, power supply (29.6-V rechargeable Li-Polymer battery pack with a capacity of 1200 mA·h), control circuits, and balancing weights are appropriately placed inside the hollow forebody.

dorsoventral oscillations with peak-to-peak amplitude of approximately 0.2 BL. The resulting dolphin robot is demonstrated in Fig. 9, which measures 72-cm long, 12-cm wide (maximum, at the shoulder), 13-cm high (maximum, at the shoulder) and weighs approximately 4.7 kg.

C. Material Choice

Besides being durable and practical, a substantial amount of lightweight materials is employed to make the dolphin robot as light as possible. The main heavy-load structures are made out of Titanium alloy (TC4, equivalent to GRADE5 in American standard), while Aluminum alloy (LY12, equivalent to 2024 in American standard) and Nylon 6 are used for other light-load components. Particularly, the bevel gears of the waist and caudal joints are made of 40Cr alloy steel (equivalent to 5140 in American standard) with high frequency quenching, which can withstand strong impacts from fast-moving motors. For the convenience of installation, the two-part head shell is made of polypropylene (PP). Instead of rigid flat plates, the fluke and flippers made of PP adopt 3-D airfoil profile. Furthermore, a black compliant outer skin made of lactoprene is custom-made to protect the structures from water and also to reduce fluid drag [37].

D. Sensory and Control Configuration

The dolphin robot contains an onboard microprocessor, various types of sensors, and a wireless communication module that enable it to both process external inputs and execute control laws. Concerning the onboard sensors, an attitude heading reference system (AHRS, MicroStrain, 3DM-GX3-25) is installed in the head shell, which provides 3-D solved attitude and heading solutions coming from inertial gyroscopes and accelerometers. An absolute pressure sensor (SQsensor, CYG-515A) fixed on the lateral surface of the middle body offers depth data. The current, speeds, and positions of the waist and caudal joints, however, can be accessed from the dedicated motor controllers (MAXON, EPOS2 50/5). At the control level, a STM32F103ZET6 (STMicroelectronics, ARM Cortex-M3 MCU with 512 Kbytes Flash, 72-MHz CPU, motor control, USB and CAN) centered embedded controller featuring abundant interface and sufficient computational power is built. Currently, a real-time operating system for embedded devices, RT-Thread 0.3.3, runs on the dolphin robot. This embedded system enable us to implement closed-loop motion control aided by sensory information in real time. Specifically, the sampling rate of the control loop is 200 Hz, corresponding to a control period of 5 ms.

E. Thrust Control

With regard to the motion control of the dolphin robot, symmetrical and large-amplitude dorsoventral oscillations of the tail and fluke produce large thrust forces, while asymmetrical oscillations of tail in conjunction with biased flippers yield different maneuvers. On the one hand, a passive control strategy with variable torque actuation is proposed for the dorsoventral propulsion, where J_1 oscillates following a sinusoidal path and J_2 is passively bent with a changing torque. Actually, the passive control strategy corresponds to torque control mode of motor, in which the rotating speed (i.e., frequency) is determined by the load. For simplicity, the driving torque of J_2 is denoted as $\tau_2 = -k\theta_2$, where k is the stiffness coefficient of J_2 and θ_2 is the joint angle of J_2. Fig. 10 illustrates the passive control strategy for J_2. Based on this strategy, the dolphin robot can easily control the torque of J_2 in closed loop. As can be observed, the torque of J_2 can be adjusted by altering the current of the driving motor (i.e., i_2) based on $i_2 = k_2\tau_2$.

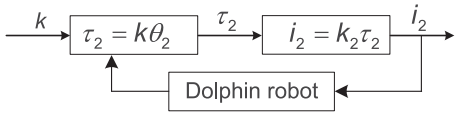

Fig. 10. Block diagram of the passive control strategy for the caudal joint.

Since the amplitude-dependent rotational angle θ_2 can directly be obtained from an encoder, the dolphin robot can use τ_2 as a feedback in terms of $\tau_2 = -k\theta_2$. To modulate the expected current, the motor controller adopts a current loop mode. Therefore, J_2 is passively oscillated with a varying torque. Notice that the optimal value of k depends on several parameters involving the oscillatory frequency and amplitude, as well as the induced propulsive speed of the robot. However, the precise propulsive speed is hardly obtained in real time. So, we empirically seek to an optimized k over a wide range of oscillatory frequencies to maximize torque and overall performance. On the other hand, closed-loop controllers responsible for separate pitch, yaw, roll, and depth controls can be built based on the feedback from onboard sensors (e.g., the AHRS and pressure sensors). Note that Proportional-Integral-Derivative (PID) algorithms are utilized in pitch, yaw, roll, and depth controls in this study. Therefore, the flexible operation of propulsive speed and the precise attitude control allows us to perform leap experiments.

IV. Experiments and Results

In order to evaluate the proposed mechatronic design and swimming performance of the developed dolphin robot, we made systematic self-propelled measurements in indoor swimming pool whose dimension is 25-m long, 10-m wide, and 1.2–1.5-m deep. The water temperature was maintained 22–26 °C. During testing, a fully charged battery pack lasted about 3.5 h. Unless otherwise specified, the data points and error bars in subsequent figures were the averages and standard deviations of five runs.

A. Experimental Results

The first experiment concerned the effect of the proposed passive control strategy on the dorsoventral propulsion. We examined the mean swimming speeds against varying oscillatory frequencies (f) and stiffness coefficients (k). To facilitate stable and convenient measurement, the dolphin robot was required to straightly travel a given distance of 4.5 m at a submerged depth of 25 cm. Prior to timing, an acceleration distance of approximately 9 m was set for the robot starting from rest. The relationship between the oscillatory frequency and the mean swimming speed under various stiffness coefficients is illustrated in Fig. 11. The mean swimming speed shows a steady increase with increasing oscillatory frequency over the entire stiffness coefficient range from 0.05 to 0.25 Nm/° with 0.05 Nm/° increments, but each stiffness coefficient related speed curve differs in slope. This inconsistency reflects the speed difference contributed by virtual stiffness associated with tail output torque at the same frequency, which in part agrees

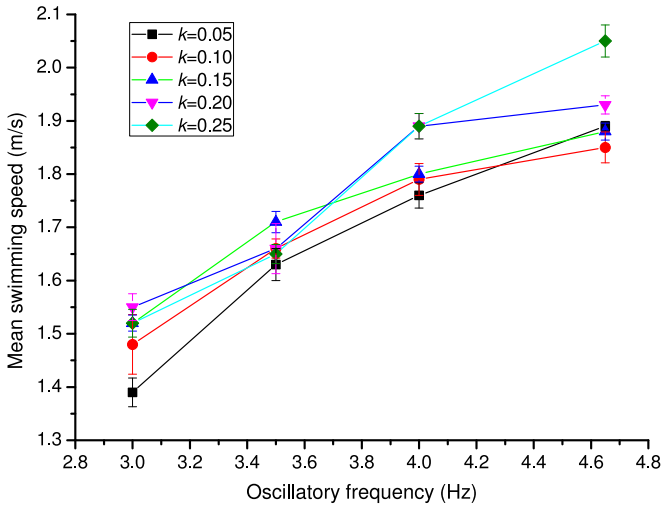

Fig. 11. Relationship between oscillatory frequency and mean swimming speed under varying stiffness coefficient conditions.

with observations of aquatic biolocomotion highlighting the important roles that both active and passive flexibility play [36]. It also suggests the stiffness coefficient should be actively tuned to maximize the propulsive speed. Generally, the dolphin robot could swim faster with increasing k at the same f. One of the main reasons is that a larger k is linked to a relatively larger attack angle of the fluke, producing larger thrust. Of course, a larger k is accompanied by relatively stronger drag. This situation results in a much stronger moment for the waist joint. Remarkably, when $k = 0.25$ Nm/°, the robot reaches a maximum swimming speed of 2.05 ± 0.03 m/s (equivalent to 2.85 BL/s, a speed previously unachieved) at $f = 4.65$ Hz. This speed corresponds to a propulsive factor of 0.61 BL/Hz, closely matching the preliminary estimation of 0.6 BL/Hz. It should be remarked that this measure of efficiency of the oscillatory motion is similar to the swimming number (Sw), which is interpreted as the distance traveled per body length during one caudal fin oscillation [10]. In such a context of efficiency measurement, the dolphin robot had a Sw of 0.61, which is close to a real dolphin's Sw (as high as 0.82, see [10]). A careful inspection also revealed that the dimensionless parameter describing the tail kinematics of swimming animals, Strouhal number, is 0.32, lying within the optimal interval between 0.2 and 0.4 for cetaceans [38].

In another experiment, we explored the possibility of performing leaps using an actual dolphin robot. The robot first initiated from rest and descended to a depth of 0.7–0.9 m at which wave drag may be completely negligible, then was made to replicate the five-phase leaping process. By increasing the initial exit speed via modulating f and k, we tried to make the robot jump out of the water. Remarkably, a complete leap was achieved when the swimming speed was higher than 1.66 m/s (approximately 2.3 BL/s, corresponding to $f = 3.5$ Hz and $k = 0.10$ Nm/°). It should be noted that the tested leaping speed of 1.66 m/s is largely consistent with the estimated $U_{0\min} = 1.62$ m/s at 60°, thus providing strong support for the

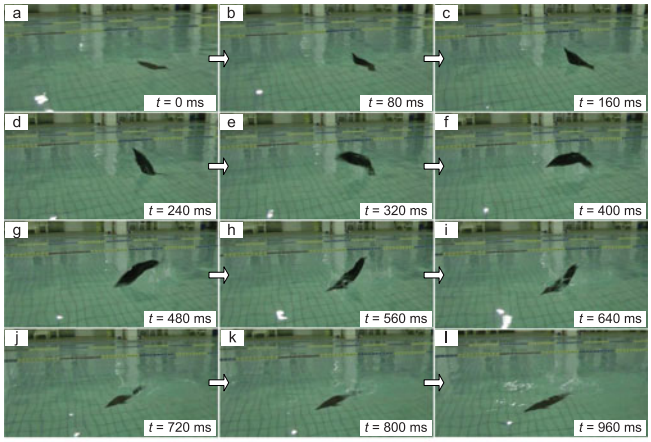

Fig. 12. Snapshot sequence of a successful dolphin leap. (a) Leap image sequence. (b) Overlaid image mainly featuring pathway of surfacing, takeoff, and reentry phases.

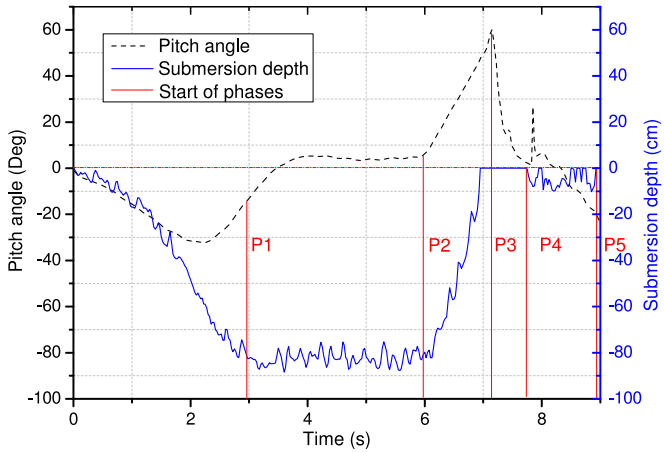

Fig. 13. Plots of pitch angle and submersion depth over time in the dolphin leap, where P1, P2, P3, P4, and P5 indicate acceleration phase, surfacing phase, takeoff phase, flight phase, and diving phase.

performed numerical estimation about the minimum exit speed. Meanwhile, as far as the absolute speed enabling leap is concerned, this critical value is much lower than the documented porpoising speeds in [12] and [13].

To the best of our knowledge, there has been no previous research on self-propelled leaping with a dolphin-like (or fish-like) robot. As an illustrative case, Fig. 12 shows a snapshot sequence of a successful leap, accompanied by the measured pitch angle and submersion depth shown in Fig. 13. Notice that the dolphin robot could leap out of the water with a height of about $1/3$–$1/2$ body lengths. Although it is far below the leaping height in live dolphins, the dolphin robot stands a good chance of faster and higher leaps through successive mechanical and control efforts. Because of space limitation, interested readers may refer to the attached experimental videos as supplementary material. As can be observed, the aerial phase lasted for more than 1 s, consistent with the biological data [39]. However, it is hard to identify the takeoff phase and the flight phase because of depth data fluctuation caused by the spray as the dolphin robot reentered. According to statistical analysis of the emergence angle data among 60 successful leaping tests, we found was varied in the range between 35° and 60°. The most frequently occurred value was around 50°. This value is significantly larger than the observed emergence angle of 31°–44° exhibited in biological dolphin [40]. This is primarily because the first priority for robot leaping is not to seek the maximum leap distance presented in the energy-conserving explanations of porpoising behavior [11], but to pursue a successful leap representing a tradeoff between the leap-height and the remaining forward speed.

B. Discussion

The attempts at obtaining high swimming speeds and taking a leap with the dolphin robot have demonstrated the effectiveness of the proposed leaping speed estimation model and mechatronic design. In general, dolphin leaping is considered as an amazing behavior and its robotic implementation as a daunting task. Now, we demonstrate that a dolphin robot is able to jump out of the water with lower speeds than expected. Specifically, by means of numerical estimation of the minimum exit speed in the framework of a rigid body model, we first obtain the relationship of minimum exit speed, body length, and emergence angle, which provides a useful guide to mechanism design and power estimation in the context of biorobotics. Then, we build a dolphin robot using commercially available parts. Furthermore, through extensive tests, we show that the dolphin robot is able to achieve leap motions above a certain exit speed (equivalent to 2.3 BL/s) that agrees well with the estimated minimum exit speed. The experimental results highlight the good model consistency. Compared with the previously reported dolphin robots in [16]–[26], whose maximum propulsive speeds are around 1 BL/s, the built dolphin robot has the following advantages for leaping motions. First, as opposed to nearly cylinder body used in dolphin robots [19], [20], [26], a well-streamlined body that is modeled after spotted dolphin gives rise to a better hydrodynamic performance. Second, a high power-to-weight ratio is chosen to produce a high propulsive speed. In general, other dolphin robots always have a relatively low power-to-weight ratio. Specifically, the dolphin robots in [16], [19], [25], and [26] have similar weights yet with lower power drivers, while the ones in [17], [18], and [20]–[22] have similar power yet with larger weight. Third, more sensors including attitude and depth sensors are well equipped to facilitate leaping control. At last, more DOFs are configured for better maneuverability and attitude control. In contrast with the dolphin robots with fixed pectoral fins [16], [19], [24]–[26], the dolphin robot possesses a

pair of 2-DOF mechanical flippers for better attitude adjustment and a neck joint for flexible control over the leaping angle of the head. Because of such features, our dolphin robot is endowed with a greater speed (as high as 2.85 BL/s) and hence a remarkable leaping capability. With the achievement of leaping ability, we may reconsider how to optimize this high-maneuverability motion and further apply it to real-world situations. For instance, the dolphin robot may jump out of the water while traveling to get a better view of distant objects on the water surface or to escape potential dangers during task execution. As a consequence, a hybrid use of underwater swimming and cross-interface leaping could be proposed as an alternative to specific underwater missions requiring both high speeds and maneuverability.

Another issue to mention is swimming performance. In terms of speed and agility, the attained performance of the dolphin robot is still far behind that of live dolphins. The relatively simple propulsive configuration and control strategies may be the main reason for the inability of the dolphin robot to overtake its biological counterpart at the moment. Thereby, more cooperative efforts on mechanics, material, actuator, sensor, control, as well as learning aspects will be demanded to enhance robotic locomotor skills in unstructured and dynamic environments. For instance, on the one hand, we may increase maximum propulsive velocity by coordinating the full-body length of the carangiform locomotion [41], [42] or using a variable stiffness mechanism [18]. On the other hand, we may use learning control method to closely mimic swimming kinematics or control mechanisms of biological counterparts [43]–[45]. With such continuous improvement efforts, the dolphin robot will attain extraordinary performance at a level comparable with live dolphins, followed by significant expansion of real-world aquatic applications.

V. Conclusion and Future Work

In this paper, we have successfully developed a bioinspired dolphin robot capable of leap motions that are characterized by both high speed and high maneuverability. We first carry out numerical estimation of the minimum exit speed so that the relationship of minimum exit speed, body length, and emergence angle is obtained. Then, based on an overall consideration of various factors involving streamlining, material, mechanism design, and passive control strategy, a fully untethered robotic prototype is created. Aquatic experiments eventually validate the effectiveness of the proposed estimation model, mechatronic design, and control strategy. We are the first to demonstrate that a self-propelled dolphin robot is able to leap out of the water.

For the purpose of enhancing the propulsive speed and maneuverability continuously, we will focus on mechanical design optimization and adaptive or learning-based tuning of control parameters for the dolphin robot by using some optimization techniques [46], [47] in our future work.

Acknowledgements

The authors would like to thank C. M. Wei, F. H. Sun, and J. D. Xiao for their assistance in preparing and performing numerous aquatic tests; Prof. F. E. Fish for his valuable suggestions on developing the dolphin robot; and the anonymous reviewers and the Technical Editor for their valuable comments and suggestions on revising this paper.

References

[1] D. T. Roper, S. Sharma, R. Sutton, and P. Culverhouse, "A review of developments towards biologically inspired propulsion systems for autonomous underwater vehicles," *J. Eng. Maritime Environ.*, vol. 225, no. 2, pp. 77–96, 2011.

[2] C. Zhou and K. H. Low, "Design and locomotion control of a biomimetic underwater vehicle with fin propulsion," *IEEE/ASME Trans. Mechatronics*, vol. 17, no. 1, pp. 25–35, Feb. 2012.

[3] L. Wen, T. Wang, G. Wu, and J. Liang, "Quantitative thrust efficiency of a self-propulsive robotic fish: Experimental method and hydrodynamic investigation," *IEEE/ASME Trans. Mechatronics*, vol. 18, no. 3, pp. 1027–1038, Jun. 2013.

[4] Z. Su, J. Yu, M. Tan, and J. Zhang, "Implementing flexible and fast turning maneuvers of a multijoint robotic fish," *IEEE/ASME Trans. Mechatronics*, vol. 19, no. 1, pp. 329–338, Feb. 2014.

[5] R. Du, Z. Li, K. Youcef-Toumi, and P. V. y Alvarado, *Robot Fish: Bio-Inspired Fishlike Underwater Robots*. Berlin, Germany: Springer-Verlag, 2015.

[6] J. Yu, F. Sun, D. Xu, and M. Tan, "Embedded vision guided 3-D tracking control for robotic fish," *IEEE Trans. Ind. Electron.*, vol. 63, no. 1, pp. 355–363, Jan. 2016.

[7] J. Yu, C. Wang, and G. Xie, "Coordination of multiple robotic fish with applications to underwater robot competition," *IEEE Trans. Ind. Electron.*, vol. 63, no. 2, pp. 1280–1288, Feb. 2016.

[8] F. E. Fish and C. A. Hui, "Dolphin swimming–A review," *Mammal Rev.*, vol. 21, no. 4, pp. 181–195, Apr. 1991.

[9] F. E. Fish and J. J. Rohr, "Review of dolphin hydrodynamics and swimming performance," U.S. Navy, San Diego, CA, Tech. Rep. 1801, Aug. 1999.

[10] M. Nagai, *Thinking Fluid Dynamics With Dolphins*. Tokyo, Japan: Ohmsha, 2002.

[11] D. W. Au and D. Weihs, "At high speeds dolphins save energy by leaping," *Nature*, vol. 284, no. 5756, pp. 548–550, 1980.

[12] D. Au, M. D. Scott, and W. L. Perryman, "Leap-swim behavior of "porpoising" dolphins," *Cetus*, vol. 8, pp. 7–10, 1988.

[13] J. J. Rohr, F. E. Fish, and J. W. Gilpatrick, "Maximum swim speeds of captive and free-ranging delphinids: Critical analysis of extraordinary performance," *Marine Mammal Sci.*, vol. 18, no. 1, pp. 1–19, 2002.

[14] J. E. Colgate and K. M. Lynch, "Mechanics and control of swimming: A review," *IEEE J. Ocean. Eng.*, vol. 29, no. 3, pp. 660–673, Jul. 2004.

[15] F. E. Fish, "Drag reduction by dolphins: Myths and reality as applied to engineered designs," *Bioinsp. Biomim.*, vol. 1, no. 2, pp. R17–R25, 2006.

[16] J. Yu, Y. Hu, R. Fan, L. Wang, and J. Huo, "Mechanical design and motion control of biomimetic robotic dolphin," *Adv. Robot.*, vol. 21, no. 3–4, pp. 499–513, 2007.

[17] P. Liu, K. He, X. Ou, and R. Du, "Mechanical design, kinematic modeling and simulation of a robotic dolphin," in *Proc. IEEE Int. Conf. Info. Autom.*, Shenzhen, China, Jun. 2011, pp. 738–743.

[18] Y.-J. Park, D. Park, and K.-J. Cho, "Design and manufacturing a robotic dolphin to increase dynamic performance," in *Proc. 10th Int. Conf. Ubiquitous Robot. Ambient Intell.*, Jeju, Korea, Oct. 2013, pp. 76–77.

[19] J. Yu, Z. Su, M. Wang, M. Tan, and J. Zhang, "Control of yaw and pitch maneuvers of a multilink dolphin robot," *IEEE Trans. Robot.*, vol. 28, no. 2, pp. 318–329, Apr. 2012.

[20] F. Shen, C. Wei, Z. Cao, C. Zhou, D. Xu, and W. Zhang, "Water quality monitoring system based on robotic dolphin," in *Proc. 8th World Congr. Intell. Contr. Autom.*, Taipei, Taiwan, Jun. 2011, pp. 243–247.

[21] M. Nakashima and K. Ono, "Development of a two-joint dolphin robot," in *Neurotechnology for Biomimetic Robots*, J. Ayers, J. L. Davis, and A. Rudolph, Eds. Cambridge, MA, USA: MIT Press, 2002.

[22] M. Nakashima, Y. Takashi, T. Tsubaki, and K. Ono, "Three-dimensional maneuverability of the dolphin robot," in *Bio-mechanisms of Swimming and Flying*, N. Kato, J. Ayers, and H. Morikawa Eds. Berlin, Germany: Springer-Verlag, 2004, pp. 79–92.

[23] G. Dogangil, E. Ozcicek, and A. Kuzucu, "Modeling, simulation, and development of a robotic dolphin prototype," in *Proc. IEEE Int. Conf. Mechatronics Autom.*, Niagara Falls, Canada, Jul. 2005, pp. 952–957.

[24] J. Yu, Y. Hu, J. Huo, and L. Wang, "Dolphin-like propulsive mechanism based on an adjustable Scotch yoke," *Mech. Mach. Theory*, vol. 44, no. 3, pp. 603–614, 2009.
[25] J. Yu, M. Wang, M. Tan, and J. Zhang, "Three-dimensional swimming," *IEEE Robot. Autom. Mag.*, vol. 18, no. 4, pp. 47–58, Dec. 2011.
[26] J. Yu and C. Wei, "Towards development of a slider-crank centered self-propelled dolphin robot," *Adv. Robot.*, vol. 27, no. 12, pp. 971–977, 2013.
[27] D. Weihs, "Dynamics of dolphin porpoising revisited," *Integ. Comp. Biol.*, vol. 42, no. 5, pp. 1071–1078, 2002.
[28] T. Sugimoto, "Revisiting the energetics of porpoising in penguins," *Theor. Appl. Mech. Jpn.*, vol. 57, pp. 331–338, 2009.
[29] Y. Wang, J. Yu, and J. Zhang, "Modelling and simulation of porpoising for a multilink dolphin robot," in *Proc. IEEE Int. Conf. Robot. Biomim.*, Phuket, Thailand, Dec. 2011, pp. 2131–2136.
[30] M. J. Lighthill, "Note on the swimming of slender fish," *J. Fluid Mech.*, vol. 9, no. 2, pp. 305–317, 1960.
[31] P. W. Webb, "Hydrodynamics and energetics of fish propulsion," *Bull. Fish. Res. Board Canada*, vol. 190, pp. 1–159, 1975.
[32] F. E. Fish, P. Legac, T. M. Williams, and T. Wei, "Measurement of hydrodynamic force generation by swimming dolphins using bubble DPIV," *J. Exp. Biol.*, vol. 217, no. 2, pp. 252–260, 2014.
[33] *NACA 0018 (naca0018-il)*. (2015). [Online]. Available: http://airfoiltools.com/airfoil/details?airfoil=naca0018-il
[34] *Pantropical Spotted Dolphin (Stenella attenuata)*. (2015). [Online]. Available: http://www.nsrl.ttu.edu/tmot1/stenatte.htm
[35] T. G. Lang and K. Pryor, "Hydrodynamic performance of porpoises (Stenella attenuata)," *Science*, vol. 152, no. 3721, pp. 531–533, 1966.
[36] F. E. Fish and G. V. Lauder, "Passive and active flow control by swimming fishes and mammals," *Annu. Rev. Fluid Mech.*, vol. 38, pp. 193–224, 2006.
[37] J. Yu, L. Wang, and M. Tan, "Geometric optimization of relative link lengths for biomimetic robotic fish," *IEEE Trans. Robot.*, vol. 23, no. 2, pp. 382–386, Apr. 2007.
[38] J. J. Rohr and F. E. Fish, "Strouhal numbers and optimization of swimming by odontocete cetaceans," *J. Exp. Biol.*, vol. 207, no. 10, pp. 1633–1642, 2004.
[39] B. Wursig and H. Whitehead, "Aerial behavior," in *Encyclopedia of Marine Mammals*, 2nd ed. W. F. Perrin, B. Wursig, and J. G. M. Thewissen, Eds. New York, NY, USA: Academic, 2009, pp. 5–11.
[40] C. A. Hui, "Surfacing behavior and ventilation in free-ranging dolphins," *J. Mammal.*, vol. 70, no. 4, pp. 833–835, 1989.
[41] R. J. Clapham and H. Hu, "iSplash-I: High performance swimming motion of a carangiform robotic fish with full-body coordination," in *Proc. IEEE Int. Conf. Robot. Autom.*, Hong Kong, May 2014, pp. 322–327.
[42] R. J. Clapham and H. Hu, "iSplash-II: Realizing fast carangiform swimming to outperform a real fish," in *Proc. IEEE/RSJ Int. Conf. Intell. Robot. Syst.*, Chicago, IL, USA, Sep. 2014, pp. 1080–1086.
[43] Z. Pan, Y. Zhang, and S. Kwong, "Efficient motion and disparity estimation optimization for low complexity multiview video coding," *IEEE Trans. Broadcast.*, vol. 61, no. 2, pp. 166–176, Jun. 2015.
[44] X. Wen, L. Shao, Y. Xue, and W. Fang, "A rapid learning algorithm for vehicle classification," *Inf. Sci.*, vol. 295, no. 1, pp. 395–406, 2015.
[45] D. Fang, C. Jie, and C. Chen, "Adaptive unscented Kalman filter for parameter and state estimation of nonlinear high-speed objects," *J. Syst. Eng. Electron.*, vol. 24, no. 4, pp. 655–665, 2013.
[46] T. Hu, K. H. Low, L. Shen, and X. Xu, "Effective phase tracking for bioinspired undulations of robotic fish models: A learning control approach," *IEEE/ASME Trans. Mechatronics*, vol. 19, no. 1, pp. 191–200, Feb. 2014.
[47] X. Niu, J. Xu, Q. Ren, and Q. Wang, "Locomotion learning for an anguilliform robotic fish using central pattern generator approach," *IEEE Trans. Ind. Electron.*, vol. 61, no. 9, pp. 4780–4787, Sep. 2014.

Junzhi Yu (SM'14) received the B.E. degree in safety engineering, and the M.E. degree in precision instruments and mechanology from the North China Institute of Technology, Taiyuan, China, in 1998 and 2001, respectively, and the Ph.D. degree in control theory and control engineering from the Institute of Automation, Chinese Academy of Sciences (IACAS), Beijing, China, in 2003.

He is currently a Professor with the State Key Laboratory of Management and Control for Complex Systems, IACAS. His research interests include biomimetic robots, intelligent control, and intelligent mechatonic systems.

Dr. Yu serves as the Associate Editor of the IEEE TRANSACTIONS ON ROBOTICS and the *Journal of Mechanical Science and Technology*, and as the Technical Editor of the IEEE/ASME TRANSACTIONS ON MECHATRONICS.

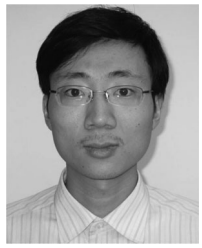

Zongshuai Su received the B.Sc. degree in automation from the School of Mathematics and System Sciences, Shandong University, Jinan, China, in 2007, and the Ph.D. degree in control theory and control engineering from the Institute of Automation, Chinese Academy of Sciences (IACAS), Beijing, China, in 2012.

He is currently an Assistant Professor with the State Key Laboratory of Intelligent Control and Management of Complex Systems, IACAS. His research interests include fast and agile maneuvers of bioinspired robotic fish and dolphins.

Zhengxing Wu received the B.E. degree in logistics engineering from the School of Control Science and Engineering, Shandong University, Jinan, China, in 2008, and the Ph.D. degree in control theory and control engineering from the Institute of Automation, Chinese Academy of Sciences (IACAS), Beijing, China, in 2015.

He is currently an Assistant Professor with the State Key Laboratory of Intelligent Control and Management of Complex Systems, IACAS. His research interests include fast maneuvers of bioinspired robotic fish and gliding motions of robotic dolphins.

Min Tan received the B.Sc. degree from Tsinghua University, Beijing, China, in 1986, and the Ph.D. degree from the Institute of Automation, Chinese Academy of Sciences (IACAS), Beijing, China, in 1990, both in control science and engineering.

He is currently a Professor with the State Key Laboratory of Management and Control for Complex Systems, IACAS. He has published more than 200 papers in journals, books, and conference proceedings. His research interests include robotics and intelligent control systems.